Korean J. Chem. Eng., **31**(8), 1470-1479 (2014)
DOI: 10.1007/s11814-014-0086-3

pISSN: 0256-1115
eISSN: 1975-7220

New carbon composite adsorbents for the removal of textile dyes from aqueous solutions : Kinetic, equilibrium, and thermodynamic studies

Davis Castro dos Santos*, Matthew Ayorinde Adebayo,***, Simone de Fátima Pinheiro Pereira*, Lizie Daniela Tentler Prola**, Renato Cataluña**, Eder Cláudio Lima*,†, Caroline Saucier**, Caline Rodrigues Gally**, and Fernando Machado Machado******

*Institute of Exact and Natural Sciences, Federal University of Para, UFPA, Belem, PA, Brazil
**Institute of Chemistry, Federal University of Rio Grande do Sul, UFRGS, Av. Bento Gonçalves 9500, Postal Box 15003, ZIP 91501-970, Porto Alegre, RS, Brazil
***Department of Chemical Sciences, Ajayi Crowther University, PMB 1066, Oyo, Oyo State, Nigeria
****Universitary Center Franciscano, UNIFRA, R. dos Andradas 1614, ZIP 97010-032, Santa Maria, RS, Brazil
(*Received 9 January 2014 • accepted 18 March 2014*)

Abstract−New carbon composite materials were prepared by pyrolysis of mixture of coffee wastes and red mud at 700 °C with the inorganic : organic ratios of 1.9 (CC-1.9) and 2.2 (CC-2.2). These adsorbents were used to remove reactive orange 16 (RO-16) and reactive red 120 (RR-120) textile dyes from aqueous solution. The CC-1.9 and CC-2.2 materials were characterized using Fourier transform infrared spectroscopy, Nitrogen adsorption/desorption curves, scanning electron Microscopy and X-ray diffraction. The kinetic of adsorption data was fitted by general order kinetic model. A three-parameter isotherm model, Liu isotherm model, gave the best fit of the equilibrium data (298 to 323 K). The maximum amounts of dyes removed at 323 K were 144.8 (CC-1.9) and 139.5 mg g^{-1} (CC-2.2) for RO-16 dye and 95.76 (CC-1.9) and 93.80 mg g^{-1} (CC-2.2) for RR-120 dye. Two simulated dyehouse effluents were used to investigate the application of the adsorbents for effluent treatment.

Keywords: Adsorption, Aqueous Effluents, Carbon Composite, General Order Kinetic Model, Pyrolysis

INTRODUCTION

As the demand for industrial products is a function of population growth, the demand for industrial products gradually increases. Dyes are coloring agents used by many industries, such as textiles, paper and pulp mills, cosmetics, food, leather, rubber, among others, for coloring their final products. The aftermath of the consumption of these products leads to the formation of wastewater contaminated with dyes. Textile industries make use of 35% of reactive dyes [1]. Cotton fiber occupies the number one position among all dyed textile fibers, and not less than 50% of cotton production utilise reactive dyes [2]. It is estimated that about 10 to 60% of reactive dyes are lost during textile dyeing, thereby generating large amounts of colored wastewater [1]. The dye-containing wastewater discharged from these industries unfavorably affect the aquatic environment, obstructing light penetration, as a result, preventing the photosynthesis of aqueous flora [3,4]. Allergy, dermatitis, skin irritation [5] and cancer and mutation in humans [6-8] have been linked to consequential impact of dyes in the environment. Treatment of reactive dye effluents is a herculean task because reactive dyes possess a complex aromatic molecular structure. This characteristic makes reactive dyes more stable and difficult for being biodegraded [9, 10]. Due to stringent of global regulations [1], the effluents from the textile industry have to be treated carefully before being discharged into the environment [11,12]. This regulation has led to an increase in demand and quest for eco-friendly technologies to remove dyes from aqueous effluents [13,14].

One of the important unitary operations for the removal of synthetic dyes from wastewaters is the adsorption process [15,16]. Adsorption is preferable because of its simplicity and high efficiency, as well as the availability of a wide range of adsorbents [17,18]. This process transfers the contaminant from the effluent to a solid phase, thereby decreasing the bioavailability of the hazardous specie to living organisms [19,20], since the toxicity of dye dissolved in water is much higher than it loaded in a solid surface [7,21]. The treated effluent can then be released to the environment [21,22]; alternatively, the water could be reused in some industrial processes that do not require water of high purity [2]. Subsequently, the adsorbents can be regenerated or stored in a dry place without direct contact with the environment [14,18,21].

Activated carbon is one of the most employed adsorbents for adsorption of organic compounds simply because it has well-developed pore structures with high specific area that favors high adsorption ability [23,24]. Moreover, the effectiveness of activated carbon to adsorb toxic species depends on the nature of organic material used for the generation of the activated carbon [24], as well as the experimental conditions employed in the activation processes [24]. Conventionally activated carbons are prepared using a number of chemical [25] and physical [26] activation methods. A combination of the chemical and physical methods is used in some cases [27].

Red mud is a residue generated from the refining of bauxite for alumina (Al_2O_3) production [28]. For every ton of Al_2O_3 produced,

†To whom correspondence should be addressed.
E-mail: eder.lima@ufrgs.br, profederlima@gmail.com

approximately one to two tons of red mud are generated [29]. Red mud is a highly alkaline waste material with pH 10-13. Due to the alkaline nature and the chemical and mineralogical species present in red mud, this solid waste has a significant impact on the environment, and proper disposal of waste red mud presents a huge challenge where aluminum industries are installed [28,29]. As red mud is a residue, it has been studied as low-cost adsorbent for removal of dyes from aqueous solutions in several applications [28-31].

Brazil produces large amounts of organic wastes (such as coffee wastes), and in 2012, Brazil emerged as the third highest annual producer of aluminum in the world, corresponding to 14.3% with a production of 31,768 10^3 ton of Al [32]. It could be estimated that at least, 31,768 10^3 tons of red mud were produced. This work is the first attempt that looks into the production of carbon composite adsorbent by a pyrolysis of the mixture of coffee wastes and red mud at 700 °C with the inorganic : organic ratios of 1.0 (CC-1.0) to 2.2 (CC-2.2). These adsorbent materials were tested for removal of reactive orange 16 (RO-16) and reactive red 120 (RR-120) textile dyes from aqueous solutions. These two dyes chosen are largely used in Brazil for dying textiles [3,23]. Carbon composite adsorbents are a mixture of organic carbonaceous material with inorganic components. This adsorbent material is different from activated carbon, because it presents the organic matrix plus the inorganic components. The aim of producing carbon composite using coffee wastes and red mud is to improve the sorption capacity of the adsorbent for dye removal in relation to only carbonized materials as well as the inorganic red mud residue.

MATERIALS AND METHODS

1. Solutions and Reagents

For preparation of solutions, deionized water was used throughout the experiments. The textile dyes, C.I. Reactive Orange 16 (RO-16 C.I. 17757; CAS 20262-58-2; $C_{20}H_{17}N_3O_{11}S_3Na_2$, 617.54 g mol^{-1}, λ_{max}=493 nm) at 50% purity and C.I. Reactive Red 120 dye (RR-120, C.I. 25810; $C_{44}H_{24}Cl_2N_{14}O_{20}S_6Na_6$, 1,469.98 g mol^{-1}) at 70% purity, were supplied by Sigma-Aldrich (St. Louis, M.O. USA). The dyes were used without further purification. The molecular structures of RO-16 and RR-120 are shown in Fig. 1(a) and Fig. 1(b), respectively. The RO-16 has one sulfato-ethyl-sulfone group and one sulfonate group while the RR-120 has six sulfonate groups. These groups exhibit negative charges even in highly acidic solutions because they possess pK_a values that are lower than zero [33].

A stock solution of 1.00 g L^{-1} was prepared by accurately weighing a calculated amount of dye and dissolving in distilled water. Various solutions for experimental work were prepared by diluting the stock solution of the dye to the required concentrations. A 0.10 mol L^{-1} sodium hydroxide solution or 0.10 mol L^{-1} hydrochloric acid solution was used to adjust the pH of the solutions. Schott Lab 850 set pH meter was used for measurement of the pH of the solutions.

2. Preparation and Characterisation Carbon Composite Adsorbents

Carbon composite adsorbents were prepared using the following procedures: A 40.0 g of inorganic matrix (71.5% red mud+21.5% lime+7.0% KOH) was mixed with a 40.0 g of coffee wastes making an inorganic : organic weight ratio of 1.0 (CC-1.0). A 35 mL of distilled water was added to the mixture to obtain a homogeneous paste. This paste was placed in a mold disc of 6 cm diameter with a thickness of 0.7 cm. Subsequently, the resulting material was wet-shaped and dried at room temperature overnight and thereafter dried in an oven at 120 °C for 10 h. Subsequently, up to 9 dried discs were placed in a cage-like structure inside the stainless reactor (see Supplementary Fig. 1) to allow a symmetric gas distribution and ensure a homogeneous gas rate (argon at 100 mL/min) around them, in

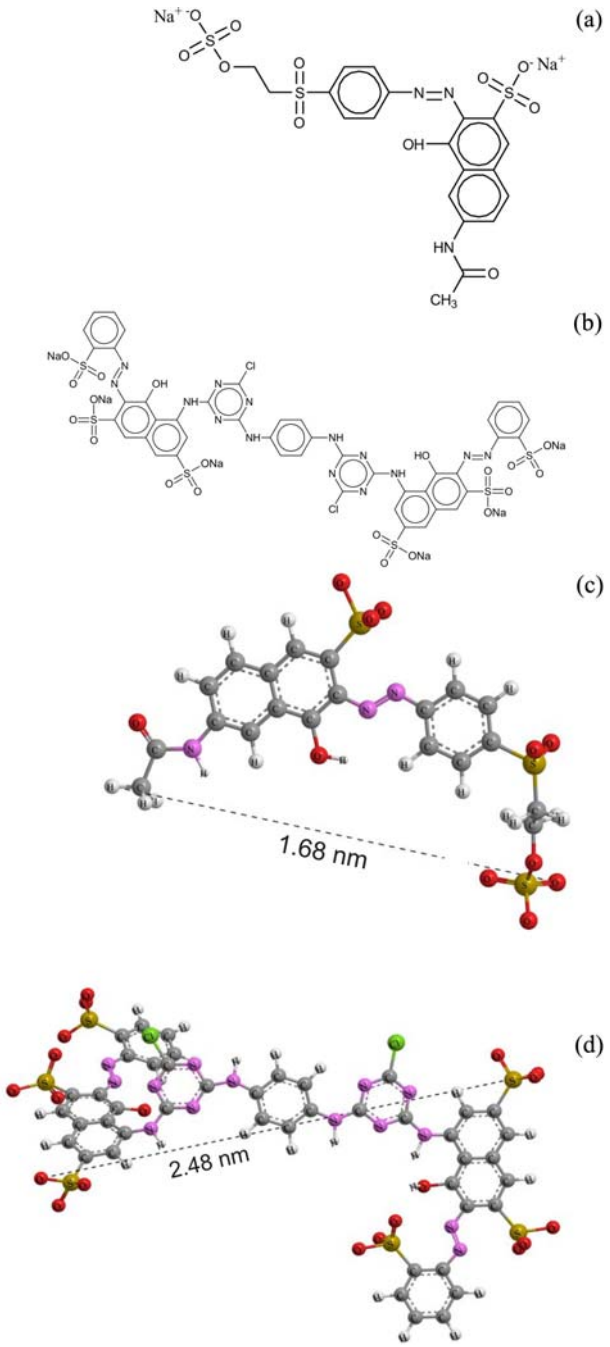

Fig. 1. Structural formulae of (a) RO-16 and (b) RR-120 dye. Optimized three-dimensional structural formulae of (c) RO-16 and (d) RR-120. The dimensions of the chemical molecule were calculated using ChemBio 3D ultra version 12.0. For respective RO-16 and RR-120, Connolly accessible area= 7.85 and 14.86 nm^2; connolly molecular area=4.29 and 8.83 nm^2; Connolly solvent excluded volume 0.380 and 0.830 nm^3.

order to avoid formation of heterogeneous carbon composite adsorbents. The reactor inside the tubular furnace was then heated at 20 °C min^{-1} up to 700 °C, remaining at this temperature for 30 minutes. Subsequently the adsorbent material was cooled to room temperature under argon (25 mL/min). The carbonized discs were then milled and sieved to particle size 125 μm, and stored in an appropriate flask. This carbon composite adsorbent was named as CC-1.0. Other carbon materials were prepared in a similar way with the inorganic : organic ratio of 1.3 (CC-1.3); 1.6 (CC-1.6); 1.9 (CC-1.9); 2.2 (CC-2.2). For comparison of sorption capacities, a carbonized material was prepared without inorganic compounds, named as C-0, and the red mud material without carbon fraction was named RM.

The carbon composite adsorbents were characterized to obtain their morphologies by employing scanning electron microscopy (SEM) using a JEOL microscope, model JSM 6060 (Tokyo, Japan) [34].

The carbon composite adsorbents were also characterized using vibrational spectroscopy in the infrared region with Fourier Transform (FTIR) with the aid of a spectrometer Shimadzu model IR Prestige 21 (Kyoto, Japan). Carbon composites and KBr were previously dried at 120 °C for 8 h, stored in capped flasks and kept in a desiccator before the analysis. The spectra were obtained with a resolution of 4 cm^{-1} using 100 cumulative scans [35].

The N_2 adsorption-desorption isotherms of CC-1.9 and CC-2.2 samples were carried out at liquid nitrogen boiling point (77 K), using a Nova 1000 surface analyser, using Quantachrome instruments. Previously, the samples were degassed for 4 h at 140 °C under vacuum. The specific surface areas were evaluated using the BET (Brunauer, Emmett and Teller) multipoint technique [35] and the pore size distribution was obtained by using the BJH (Barrett, Joyner and Halenda) method [36].

The CC-1.9 was characterized by X-ray diffraction (XRD) with a Philips X'pert MPD diffractometer (Netherlands) operating at 40 kV and 40 mA with Cu Kα radiation (λ=1.5406 Å). Measurements were done with scanning step width of 0.05° and time of 3 s, over the 2θ range of 5-75° [11].

3. Adsorption Studies

The batch adsorption studies for probing the ability of carbon composite adsorbents to remove RO-16 and RB-120 dyes from aqueous solutions were carried out in triplicate, using a standard batch adsorption method. A 50.0 mg of adsorbent was placed in 50 ml flat-bottom Falcon tubes containing 20.0 ml of dye solution (10.00 to 300.0 mg L^{-1}), which were agitated for an appropriate time (0.0833 to 10.00 h) using an acclimatized shaker (Oxylab, São Leopoldo, Brazil) at temperatures ranging from 298 to 323 K. The pH of the dye solutions ranged from 2.0 to 10.0. Immediately after the batch adsorption experiments, the tubes containing adsorbent and adsorbate were centrifuged at 10,000 rpm for 5 min using a Unicen M Herolab centrifuge (Stuttgart, Germany) so as to to separate the adsorbents from the aqueous solutions. Aliquots of 1-10 mL of the supernatant were properly diluted with de-ionized water adjusted to pH 2.0.

The final concentrations of the residual dyes in the solution were measured by visible spectrophotometry with a T90+ UV-VIS spectrophotometer (PG Instruments, London, United Kingdom) fitted with quartz optical cells. Absorbance measurements of RO-16 and RR-120 dyes were made at maximum wavelength of 489 and 534 nm, respectively.

The amount of dye removed by the adsorbents and the corresponding percentage of removal were calculated with the aid of Eqs. (1) and (2), respectively:

$$q = \frac{(C_o - C_f)}{m} \cdot V \quad (1)$$

$$\%\text{Removal} = 100 \cdot \frac{(C_o - C_f)}{C_o} \quad (2)$$

where, q is the amount of dye adsorbed by the adsorbent in mg g^{-1}, C_o is the initial dye concentration in contact with the adsorbent (mg L^{-1}), C_f is the dye concentration (mg L^{-1}) after the batch adsorption process, m (g) is the mass of adsorbent and V is the volume of dye solution (L).

4. Quality Assurance, and Statistical Evaluation of the Kinetic and Isotherm Parameters

All the experiments were done in triplicate to establish the reliability, reproducibility and accuracy of the experimental data. The relative standard deviations of all measurements were less than 5% [37]. Blank tests were run in parallel and corrected when necessary [38].

All dye solutions were stored in airtight glass flasks, which were cleaned by being immersed in 1.4 mol L^{-1} HNO_3 for 24 h [39], rinsed several times with de-ionized water, dried and stored in a flow-hood.

Standard solutions of dyes with concentrations ranging from 5.00 to 130.0 mg L^{-1} were used for analytical calibration, in parallel with a blank solution of water adjusted to pH 2.0. The linear analytical calibration of the curve was done using the UVWin software of the T90+ PG Instruments spectrophotometer. The spectrophotometric detection limits for RO-16 and RR-120 dyes were 0.11 mg L^{-1} and a 0.19 mg L^{-1}, respectively, obtained with a signal/noise ratio of 3 [40]. All the analytical measurements were carried out in triplicate, and the precision of the standards was better than 3% (n=3). A 50.0 mg L^{-1} standard dye solution was employed as a quality control after every five determinations during spectrophotometric measurements for verification of the accuracies of the RO-16 and RR-120 sample solutions [36].

A nonlinear method, with successive interactions calculated by the Levenberg-Marquardt method, was used for fitting the kinetic and equilibrium data. Interactions were also calculated using the Simplex method, based on the nonlinear fitting facilities of the Microcal Origin 9.0 software. The models were evaluated using a determination coefficient (R^2), an adjusted determination coefficient (R^2_{adj}) and an error function (F_{error}) [3,4]. F_{error} is a measured of the differences between the theoretical amount of dye removed by the adsorbent and the actual the amount of dye measured experimentally. Eqs. (3), (4) and (5) are the mathematical expressions of R^2, R^2_{adj} and F_{error}, respectively.

$$R^2 = \left(\frac{\sum_i^n (q_{i,exp} - \overline{q}_{i,exp})^2 - \sum_i^n (q_{i,exp} - q_{i,model})^2}{\sum_i^n (q_{i,exp} - \overline{q}_{i,exp})^2} \right) \quad (3)$$

$$R^2_{adj} = 1 - (1 - R^2) \cdot \left(\frac{n-1}{n-p-1} \right) \quad (4)$$

$$F_{error} = \sqrt{\left(\frac{1}{n-p} \right) \cdot \sum_i^n (q_{i,exp} - q_{i,model})^2} \quad (5)$$

$q_{i,model}$ is the each theoretical value of q predicted by the model, $q_{i,exp}$ is the each value of q measured experimentally, $\overline{q}_{exp}$ is the average of q measured experimentally, n is the number of experiments performed, and p is the number of parameters in the fitting model [3,4].

5. Kinetic Adsorption Models

The kinetic equations used in this work are:

Pseudo-first order (Eq. (6)); pseudo-second-order (Eq. (7)); general-order kinetic model (Eq. (8)); and intra-particle diffusion model (Eq. (9)).

$$q_t = q_e[1-\exp(-k_1 \cdot t)] \quad (6)$$

$$q_t = q_e - \frac{q_e}{[k_2(q_e)\cdot t+1]} \quad (7)$$

$$q_t = q_e - \frac{q_e}{[k_N(q_e)^{n-1}\cdot t\cdot(n-1)+1]^{1/1-n}} \quad (8)$$

$$q_t = k_{id}\sqrt{t} + C \quad (9)$$

For further details of these models, please see Supplementary material [22,41-44].

6. Equilibrium Models

The Langmuir (Eq. (10)), Freundlich (Eq. (11)) and Liu (Eq. (12)) are the equilibrium equations used in this work.

$$q_e = \frac{Q_{max}\cdot K_L\cdot C_e}{1+K_L\cdot C_e} \quad (10)$$

$$q_e = K_F\cdot C_e^{1/n_F} \quad (11)$$

$$q_e = \frac{Q_{max}\cdot(K_g\cdot C_e)^{n_L}}{1+(K_g\cdot C_e)^{n_L}} \quad (12)$$

For further details of these models, please see Supplementary material [45-47].

7. Simulated Dye-house Effluent

Two synthetic dye-house effluents, each containing five representative textile dyes commonly used for coloring fibers and their corresponding auxiliary chemicals using a mixture of different dyes largely applied in the textile fiber industries, were prepared at pH 2.0. Based on the useful information obtained from a dye-house, 10-60% [1] of typical synthetic dyes and 100% of the dye bath auxiliaries remain in the spent dye bath, and its composition undergoes a 5-30-fold dilution during the subsequent washing and rinsing stages [3,13,14,18,21,22]. Table 1 shows the auxiliary chemicals and concentrations of various dyes selected to mimic an exhausted dye bath [3,13,14,18,21,22].

Table 1. Chemical composition of the simulated dyehouse effluents

Concentration (mg L^{-1})		
Dye	Effluent A	Effluent B
Reactive orange 16 (λ_{max} 489 nm)	20.00	5.00
Reactive red 120 (λ_{max} 534 nm)	5.00	20.00
Cibacron brilliant yellow 3G-P (λ_{max} 402 nm)	5.00	5.00
Procion blue MX-R (λ_{max} 594 nm)	5.00	5.00
Reactive black 5 (λ_{max} 598 nm)	5.00	5.00
Auxiliary chemical		
Na_2SO_4	80.0	80.0
NaCl	80.0	80.0
Na_2CO_3	50.0	50.0
CH_3COONa	50.0	50.0
CH_3COOH	300.0	300.0
pH	2.0*	2.0*

*pH of the solution adjusted with 0.10 mol L^{-1} HCl and 0.10 mol L^{-1} NaOH

RESULTS AND DISCUSSION

1. Preliminary Results and Characterization of Carbon Composite Adsorbents

Carbon composite adsorbents are a mixture of organic carbonaceous material with inorganic components. This adsorbent material is different from activated carbon, because it presents the organic matrix plus the inorganic components. Both organic mixed with inorganic enhances the sorption capacity of the adsorbent. To the best of our knowledge, this is the first paper reporting the use of carbon composite adsorbent of an organic matrix with red mud (RM) for the removal of dyes. The inorganic components used in this work were 71.5% red mud+21.5% lime+7.0% KOH. RM, the inorganic component, has already been used as a low-cost adsorbent, [28-30]

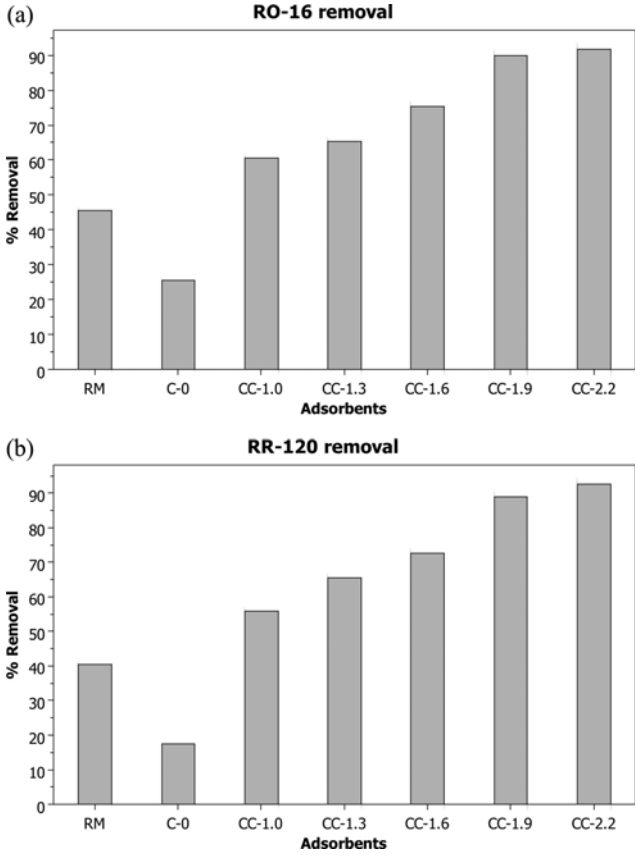

Fig. 2. Preliminary experiments of sorption capacity of different adsorbents for RO-16 and RR-120 dyes removal from aqueous solutions. The initial pH was fixed at 2.0; adsorbent mass 50.0 mg, temperature 298 K, and initial dye concentration of 50.0 mg L^{-1}.

and its use is eco-friendly since it is a hazardous environmental passive, whose contents need to be decreased. Lime was used to give garter between all the components forming the paste that was disposed in the discs (see supplementary Fig. 1). Potassium hydroxide is usually used as activating agent in the production of activated carbons [25]. Usually, the chemical activation involves the impregnation of organic matrix (solid) with aqueous solutions of inorganic salt. Then the aqueous solution is eliminated in a furnace, before the carbonization and activation. However, this procedure did not provide a homogeneous distribution of the inorganic in all the organic carbonaceous materials [25]. On the other hand, the material in the form of discs was placed in a cage-like structure inside the stainless reactor, which allowed a symmetric inert gas distribution and a more isothermal condition to the production of the carbon composite material.

Different adsorbent materials were tested for the removal of 200 mg L^{-1} of RO-16 and RR-120 dyes from aqueous solutions (see Fig. 2). As can be observed, the carbonized coffee wastes (C-0) at 700 ºC had the lowest percentage of removal of dye (<25.5% for RO-16 and <17.6% for RR-120) among all adsorbents tested. The RM exhibited percentage removal of 45.6, and 40.5 for RO-16 and RR-120 dyes, respectively. But the carbon composite formed by RM and coffee wastes presented percentage removal of at least 60.5 and 55.7% for RO-16 and RR-120 dyes, respectively. The results show that the carbon composite materials have higher sorption capacity than RM and carbonized coffee wastes alone. Since the best percentage of dye removal was attained using CC-1.9 and CC-2.2, these two adsorbent materials were chosen to continue the remaining part of the experimental work.

Table 2. Vibrational FTIR bands of CC-1.9 and CC-2.2

CC-1.9	
Band (cm^{-1})	**Assignments** (Alencar et al., 2012b; Cardoso et al., 2012; Prola et al., 2013a)
3124-3004	O-H stretch
2906	C-H asymmetric stretch
2750	C-H stretch of aldehyde
1773	C=O asymmetric stretch of ester
1727	C=O stretch of aldehyde
1630, 1431	Rings mode of aromatic
1536	C-O stretch of inorganic carbonate
1379	C-H bend of aldehyde
1244	C-O stretch of phenols
1077, 1005	C-O stretch of alcohols or Si-O stretch of silicates
895	C-O of inorganic carbonate
818, 663, 513	CH - out of plane bends of aromatic rings
CC-2.2	
3158	O-H stretch
2932	C-H asymmetric stretch
2364 and 2328	Probable CO_2 adsorbed on the sample
1810	C=O asymmetric stretch of ester
1770	C=O asymmetric stretch of ester
1654	Rings mode of aromatic
1539	C-O stretch of inorganic carbonate
1233	C-O stretch of phenols
890	C-O of inorganic carbonate
817	CH - out of plane bends of aromatic rings

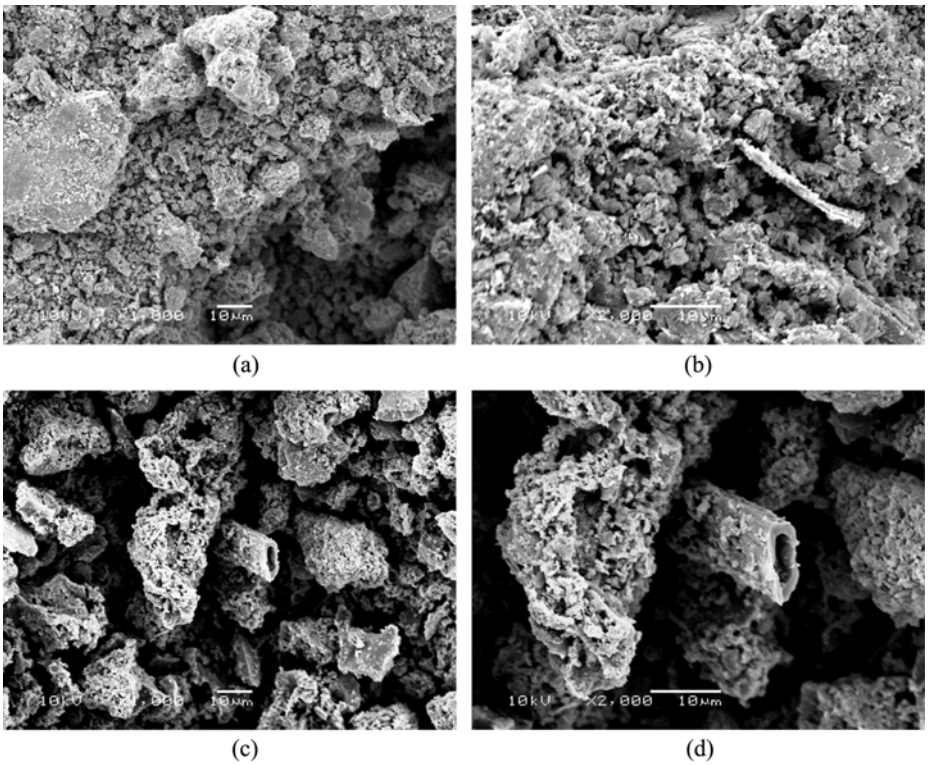

Fig. 3. Scanning electron microscopy images of: (a) 1,000 × magnification CC-1.9; (b) 2,000 × magnification CC-1.9; (c) 1,000 × magnification CC-2.2; (d) 2,000 × magnification CC-2.2.

FTIR technique was used to examine the surface groups that are present in CC-1.9 and CC-2.2 adsorbents and identify the groups responsible for adsorption of RO-16 and RR-120 dyes. Infrared spectra of the biosorbents were recorded in the range 4,000-400 cm^{-1} (Table 2). Table 2 shows the band assignments [3,14,22] of the functional groups present in CC-1.9 and CC-2.2. The functional groups present in the two carbon adsorbents are identical except for some small shifts of vibrational bands (Supplementary Fig. 2 and Table 2). The major groups found in both carbon materials include O-H (alcohols, phenols), C=O (esters and aldehydes), aromatic rings, C-O (phenols, alcohols, and inorganic carbonate), Si-O (silicates), C-H (aromatics, aliphatic chains).

The textural properties obtained using nitrogen adsorption/desorption curves are superficial area (S_{BET}), 12.3 and 6.6 $m^2\ g^{-1}$; average pore radius (BJH), 1.9 and 1.9 nm; NLDFT pore radius (Mode), 1.3 and 1.4 nm; and total pore volume, 0.11 and 0.11 $cm^3\ g^{-1}$, for CC-1.9 and CC-2.2, respectively. Supplementary Fig. 3 presents the graphs of NLDFT pore radius distribution. Although, the average pore radii of carbon materials obtained by the BJH method are a little bit higher than the values obtained by NLDFT pore as shown in Supplementary Fig. 3. It is unusual to observe that there is a presence in lower proportion of pore radius of up to 30 Å (pore diameter of 6 nm). The maximum longitudinal lengths of RO-16 and RR-120 dyes are 1.68 and 2.48 nm, respectively, as shown in Figs. 1(c) and 1(d). For these dye molecules to enter inside the pores of carbon materials, pore radius of at least 0.84 nm (8.4 Å) and 1.24 nm (12.4 Å) is required. Note that the S_{BET} of the carbon composite materials are lower when compared with activated carbons [3,23], because the inorganic components are distributed throughout the organic matrix, closing the pores of the carbon. However, the inorganic components also act as adsorbent, enhancing the sorption capacity of the adsorbent, as discussed above (see Fig. 2).

The SEM images of CC-1.9 and CC-2.2 as shown in Fig. 3 indicate that the two adsorbents have similar textural appearances. Both carbon materials lost their fibrous material characteristics after pyrolysis at 700 °C [14]. The roughness of the carbon materials is noticeable. The remarkable difference is that CC-1.9 carbon material possesses small pieces of carbon; on the other hand, CC-2.2 with lower content of inorganic matrix possesses pieces of carbon with higher dimension. Macropores (pore with ∅>50 nm) are visible in both carbon composite materials.

Supplementary Figs. 4(a) and 4(b) show the thermogravimetric profiles of CC-1.9 and CC-2.2, respectively. The thermogravimetric profiles' data of CC-1.9 and CC-2.2 are comparable with those of activated carbons already reported [23]. From 200 to 600 °C, both carbon materials have thermal stability with slightly mass loss (<3%). The decomposition of activated carbons occurs only above 600 °C [23]. Similarly, these thermograms reveal that a high content of inorganic matrix is present in both carbon materials.

X-ray diffractogram of the CC-1.9 is presented in Supplementary Fig. 5. The XRD patterns of the CC-1.9 indicate the presence of calcite. syn. (JCPDS Card 00-005-0586) in as-prepared powder, but a calcium aluminum silicate phase (JCPDS Card 00-052-1344) is also detected. These inorganic components were mixed with coffee wastes in the carbon composite preparation. The CC-2.2 diffractogram was not inserted in the manuscript, but the results are quite similar to those reported in Supplementary Fig. 5.

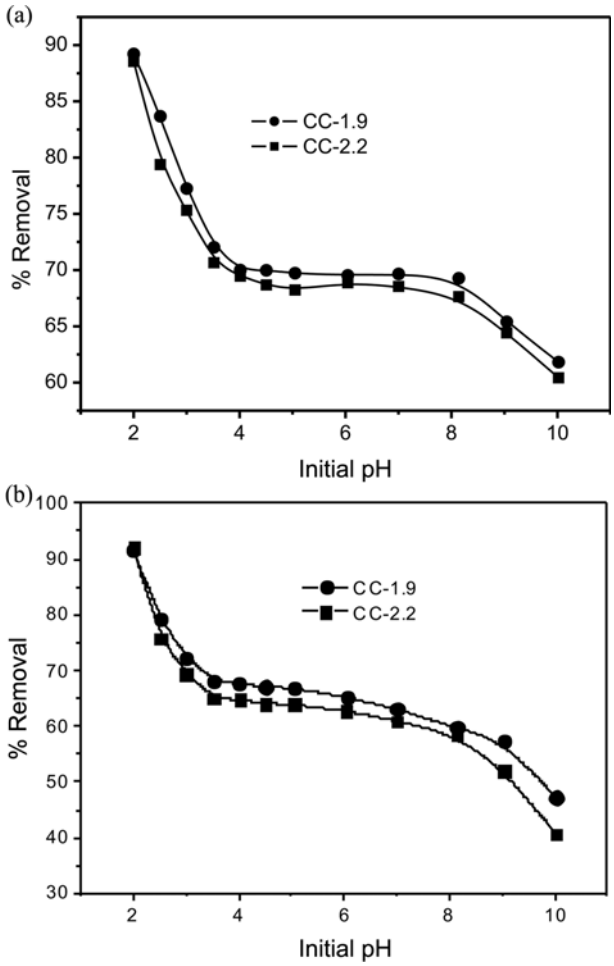

Fig. 4. Effect of initial pH on the sorption capacity. (a) RO-16; (b) RR-120. Conditions: temperature 298 K; adsorbent mass 50.0 mg; and initial dye concentration of 50.0 mg L^{-1}.

2. Effects of pH of Dye Solutions on Adsorption

The pH of the adsorbate solution is one of the influential factors affecting the adsorption of dye on an adsorbent [3,4,19]. Different dyes have different ranges of suitable pH depending on the type of adsorbent used. The effects of initial pH on percentage removal of RO-16 and RR-120 dye solutions (50 mg L^{-1}) using CC-1.9 and CC-2.2 adsorbents were investigated within the pH range of 2 and 10 (see Fig. 4). The characteristics of both dyes being adsorbed by both carbon composites were similar. The percentage of dye removal decreased from *ca* 88.2% (pH 2.0) to *ca* 68.7% (pH 7.0) for RO-16 dye. In a similar manner, the percentage of RR-120 dye removed was found to decrease from *ca* 91.5% (pH 2.0) to *ca* 61% (pH 7.0). Despite the fact that the adsorption of both dyes on the carbon composite adsorbents was favorable at initial pH of 2.0, the decrease in the percentage of dye removal is not too low when compared with agricultural residues used as biosorbent [14,19,20,22] where the decrease of percentage of dye removal could easily reach 60% [14].

Due to the observation of this pH phenomenon, other adsorption experiments of RO-16 and RR-120 dyes on CC-1.9 and CC-2.2 adsorbents were carried out at the initial pH 2.0.

3. Kinetic Studies

Nonlinear pseudo-first order, pseudo-second order and general-

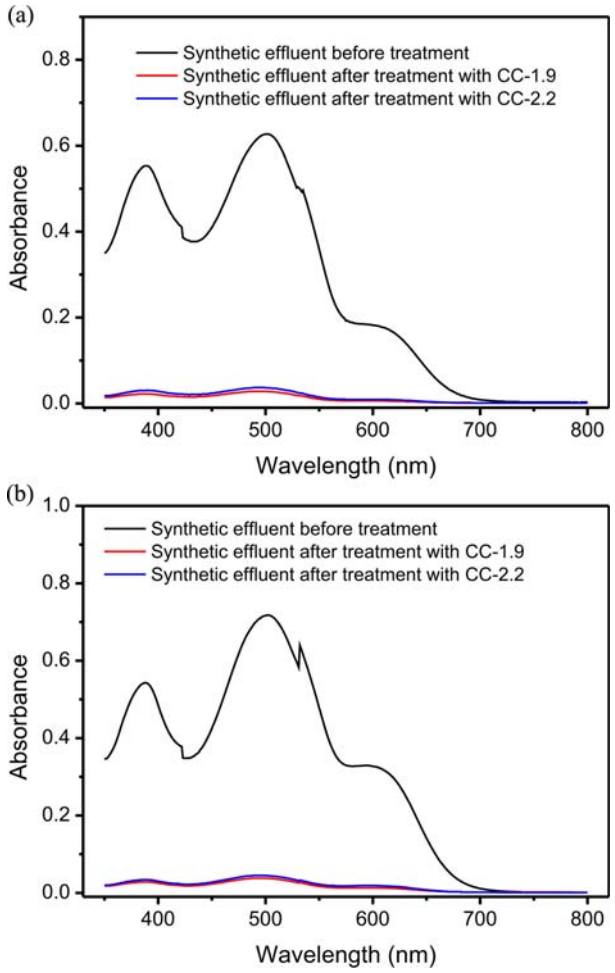

Fig. 5. UV-Vis spectra of simulated dye effluents before and after treatment with CC-1.9 and CC-2.2. (a) Effluent A; (b) Effluent B. For composition of effluents, see Table 1.

order kinetic models were used to assess the kinetics of adsorption of RO-16 and RR-120 dyes onto CC-1.9 and CC-2.2 adsorbents (Supplementary Figs. 6 and 7). Supplementary Table 1 shows the fitting parameters of the three kinetic models. Taking into consideration that the experimental data were fitted to nonlinear kinetic models, an error function (F_{error}) was used to evaluate the fit of the experimental data. The lower the F_{error}, the lower the difference between the values of q calculated theoretically and q measured experimentally (see Eq. (5)) [4,15,21,23]. Note that the F_{error} used in this work takes into account the number of fitting parameters (*p* term of Eq. (5)) since it is reported [48] that the best fit of the results depends on the number of parameters present in nonlinear equations. Thus, the number of fitting parameters should be taking into consideration while calculating the F_{error}. To compare the different kinetic models, the F_{error} of each individual model was divided by the F_{error} of the minimum value (F_{error} ratio). It was found that the F_{error} ratio values for the general order kinetic model were always 1.00. The pseudo-first order kinetic model has F_{error} ratio values ranging from 6.67 to 9.33 (CC-1.9) for the dye RO-16 and 12.51 to 12.56 (CC-2.2). Correspondingly, the pseudo-second order model has F_{error} ratio values ranging from 3.85 to 3.86 (CC-1.9) and 4.94 to 7.35 (CC-2.2). For the dye RR-120, the pseudo-first order kinetic model has F_{error} ratio values varying from 2.59 to 3.49 (CC-1.9) and 1.43 to 4.16 (CC-2.2). Similarly, the F_{error} ratio values of pseudo-second order model varied from 2.59 to 3.49 (CC-1.9) and 2.64 to 13.58 (CC-2.2). These results clearly indicate that the general-order kinetic model explains the adsorption process of RO-16 and RR-120 dyes onto CC-1.9 and CC-2.2 adsorbents better than the other two kinetic models.

Since the general-order kinetic equation takes different values of n (order of adsorption reaction) when the concentration of the adsorbate is changed (see Supplementary Table 1), it is difficult to compare the kinetic parameters of the model. In this regard, it is useful to use the initial sorption rate h_0 [43] to evaluate the kinetics of a given model by using Eq. (13).

$$h_0 = k_n \cdot q_e^n \tag{13}$$

In Eq. (13), h_0 is the initial sorption rate (mg g^{-1} h^{-1}), k_n is the rate constant [h^{-1}(g mg^{-1})$^{n-1}$], [22] q_e is the amount adsorbed at the equilibrium (mg g^{-1}), while n is the order of the kinetic model. It should be emphasized that this equation has the same initial sorption rate as when n=2 as early reported [43]. We observed that an increment in the initial dye concentration leads to an increase in the initial sorption rate for all kinetic models, as expected. This observation is an indication that there is consistency with the experimental data [3,14,18,20,22]. Since the kinetic data were better described by the general-order kinetic model, the more confident initial sorption rates (h_0) were obtained by the general order kinetic model. The general-order kinetic model expresses that the order of an adsorption process should follow the same logic as in a chemical reaction, where the order of reaction is experimentally measured [3,14,18,20,22] instead of being confined by a given model.

The kinetics of adsorption of RO-16 dye on CC-1.9 and CC-2.2 was faster than that of RR-120. Examining the ratio of initial sorption rate (h_0) of RO-16 divided by initial sorption rate of RR-120 dye, the following average rates were obtained: 3.28 (CC-1.9) and 3.57 (CC-2.2). Considering the Connolly solvent excluded volume of both dyes (Fig. 1) and making a ratio, V RR-120/V RO-16=2.18 (V stands for Connolly solvent excluded volume), hence, the dimension of the dye explains part of the difference of faster kinetics of adsorption of RO-16 compared to RR-120 dye. The lower the molecular dimension (molecular area, molecular volume) the faster the rate of reaction because the number of effective shocks between the dye molecules and the active sites of the adsorbent will be higher.

The intra-particle diffusion model [44] was also employed to ascertain the influence of mass transfer resistance on the binding of RO-16 and RR-120 dyes to the adsorbents (Supplementary Table 1 and Supplementary Figs. 8 and 9). The intra-particle diffusion constant, k_{id} (mg g^{-1} $h^{-0.5}$), is obtainable from the slope of the plot of q_t versus the square root of the time. Supplementary Figs. 8 and 9 show the plots of q_t versus $t^{1/2}$ with three linear sections for the two dyes using the CC-1.9 and CC-2.2 adsorbents. These results imply that the adsorption processes required more than one sorption rate [11,12]. Both adsorbents exhibited three stages of adsorption; each stage is attributed to each linear portion of the plots as shown in Supplementary Figs. 8 and 9. The first linear section was attributed to the process in which dye diffuses to the adsorbent surface [11,12]; hence, the fastest sorption stage. The second section was ascribed to intra-particle diffusion, a delayed process [11,12]. The third section may

be regarded as diffusion through smaller pores, followed by the establishment of equilibrium [11,12]. Looking closely at the first point of the third segment, the minimum contact time to attain the equilibrium is 4.0 h for RO-16 dye. However, for the RR-120 dye, the first point of the third linear segment is 5.0 h. These results are in good agreement with the molecular size of the dyes as discussed earlier.

The contact time used for the establishment of the equilibrium was set as 5.0 h for RO-16 and 6.0 h for RR-120 dye for the rest of our experimental work. The increment in contact time used in this work is a guarantee that equilibrium would be attained by both dyes even at higher adsorbate concentrations [18,21,23].

4. Equilibrium Studies

Adsorption isotherms describe the existing relationship between the amount of adsorbate adsorbed by the adsorbent (q_e) and the adsorbate concentration remaining in solution after the system attained equilibrium (C_e) at a constant temperature. The adsorption parameters of the equilibrium models provide some insights into the adsorption mechanism, surface properties and affinity of the adsorbent with the adsorbate. We tested the Langmuir [45], Freundlich [46], and Liu [47] isotherm models.

The isotherms of adsorption were carried out between 298 and 323 K with RO-16 and RR-120 dyes on CC-1.9 and CC-2.2 using the optimum experimental conditions previously described above (see Supplementary Table 2; Supplementary Fig. 10). Supplementary Fig. 10 shows the adsorption isotherms of RO-16 and RR-120 dyes using CC-1.9 and CC-2.2 at 323 K. Based on the F_{error} (see Supplementary Table 2), the Liu model was the best isotherm model for both biosorbents at all six experimental temperatures. The Liu model showed the lowest F_{error} values (Supplementary Table 2), indicating that the theoretical q of the isotherm model was close to the experimentally measured q.

The F_{error} of each individual model was divided by the F_{error} of minimum value (F_{error} ratio) for comparison of the different equilibrium isotherm models. The Freundlich isotherm model has F_{error} ratio values varying from 3.30 to 10.76 (CC-1.9) and 3.43 to 10.97 (CC-2.2) for RO-16 dye. Similarly, the Langmuir isotherm model has F_{error} ratio varying from 1.24 to 12.89 (CC-1.9) and from 14.96 to 34.03 (CC-2.2) for the same dye. For RR-120 dye, the Freundlich isotherm model has F_{error} ratio values ranging from 6.02 to 8.50 (CC-1.9) and 5.11 to 11.40 (CC-2.2). In the same manner for RR-120 dye, the Langmuir isotherm model has F_{error} ratio ranging from 1.19 to 14.31 (CC-1.9) and from 15.52 to 64.25 (CC-2.2). The F_{error} ratio analyses clearly indicate that the Liu isotherm model best explains the equilibrium of adsorption of RO-16 and RR-120 dye on the CC-1.9 and CC-2.2 adsorbents in the temperature range of 298 to 323 K (F_{error} ratio values always being 1.00).

The maximum amounts of RO-16 and RR-120 dyes adsorbed were 144.8 (CC-1.9) and 139.5 mg g^{-1} (CC-2.2) for RO-16 dye, and 95.76 (CC-1.9) and 93.80 mg g^{-1} (CC-2.2) for RR-120 dye at 323 K. It should be stressed that Q_{max}, the maximum amount of the RO-16 adsorbed on both adsorbents, was 48.72-51.21% higher than that of the RR-120 dye. Additionally, the kinetics of adsorption for RO-16 was 3.28 (CC-1.9) and 3.57 (CC-2.2) times faster than that of RR-120 dye on the same adsorbents. The size of the dye molecules explains why the kinetics RO-16 is faster for the two carbon composite adsorbents. The same explanation goes for higher adsorption capacity of RO-16 on the adsorbents.

5. Thermodynamics Studies

Gibb's free energy change (ΔG^o, kJ mol^{-1}), enthalpy change (ΔH^o, kJ mol^{-1}) and entropy change ($S\Delta^o$, J $mol^{-1}K^{-1}$) are thermodynamic parameters related to the adsorption process. They were evaluated using Eqs. (14)-(16).

$$\Delta G^o = \Delta H^o - T\Delta S^o \quad (14)$$

$$\Delta G^o = -RT\mathrm{Ln}(K) \quad (15)$$

Combining Eqs. (14) and (15), Eq. (16) is obtained.

$$\mathrm{Ln}(K) = \frac{\Delta S^o}{R} - \frac{\Delta H^o}{R} \times \frac{1}{T} \quad (16)$$

where R is the universal gas constant (8.314 J K^{-1} mol^{-1}), T is the absolute temperature (Kelvin) and K is the equilibrium adsorption constants of the isotherm fits (K_g- Liu equilibrium constant, which must be converted to SI units, by using the molecular mass of the dye). It has been reported in the literature that different adsorption equilibrium constants (K) were obtained from different isotherm models [3,14,15,18,20-23,41,49-51]. Thermodynamic parameters of adsorption can also be estimated from the Liu equilibrium constant, K_g [3,18,20].

The ΔH^o and ΔS^o values can be calculated from the respective slope and intercept of the linear plot of Ln(K) versus 1/T.

Table 3 shows the thermodynamic data. The R^2 values of the linear fit are ≈0.99, indicating that the values of enthalpy and entropy calculated for both adsorbents were plausible. Furthermore, the magnitude of enthalpy was consistent with a physical sorption for RO-16 and RR-120 dyes using both adsorbents [52]. To a certain level, the type of interaction can be classified by the magnitude of enthalpy change. Physical sorption, such as hydrogen bonding, is generally lower than 35 kJ mol^{-1} [52]. Enthalpy changes (ΔH^o) signify that the adsorption processes of RO-16 and RR-120 dyes using CC-1.9 and CC-2.2 adsorbents are endothermic in nature. Negative values of ΔG^o indicate that the adsorption of dyes onto CC-1.9 and CC-2.2 was spontaneous and favorable at all the experimental temperatures. The positive values of ΔS^o suggested an increased in the randomness at the solid/liquid interface. The water coordinated molecules are displaced by dye molecules and thereby gain more translational entropy than what is lost by dye molecules (this takes place during adsorption), resulting in increased randomness in the dye-adsorbent interaction [53,54].

6. Treatment of a Simulated Dye-house Effluent

Two simulated dye-house effluents were prepared (see Table 1) with different compositions of dyes and were used to investigate the effectiveness and efficiency of CC-1.9 and CC-2.2 to remove dyes from textile effluents. The UV-VIS spectra of the untreated effluents and effluents treated with CC-1.9 and CC-2.2 were recorded from 350 to 800 nm (Fig. 5). The areas under the absorption bands from 350 to 800 nm were used to monitor the percentage of the dye mixture removed from the simulated dye effluents. Both carbon adsorbents exhibited very good performance on the treatment of simulated effluents. The percentages of removal of mixture of dyes were 96.0 and 94.5% for CC-1.9 and CC-2.2, respectively, for the effluent A. For the effluent B, the corresponding percentage values were 95.0 and 94.0% for CC-1.9 and CC-2.2, respectively. These percentages are excellent when compared with published data using

Table 3. Thermodynamic parameters of the adsorption of RO-16 and RR-120 dyes on CC-1.9 and CC-2.2 adsorbents. Conditions: mass of adsorbent 50.0 mg, pH fixed at 2.0; contact time of 5 h for RO-16 and 6 h for RR-120

	Temperature (K)					
	298	303	308	313	318	323
RO-16						
CC-1.9						
K_g (L mol^{-1})	$3.42.10^3$	$4.23.10^3$	$5.29.10^3$	$6.51.10^3$	$8.11.10^3$	$1.01.10^4$
ΔG (kJ mol^{-1})	−20.16	−21.04	−21.95	−22.85	−23.80	−24.77
ΔH^o (kJ mol^{-1})	34.7	-	-	-	-	-
ΔS^o (J K^{-1} mol^{-1})	184	-	-	-	-	-
R^2	0.9991	-	-	-	-	-
CC-2.2						
K_g (L mol^{-1})	$3.66.10^3$	$4.67.10^3$	$5.84.10^3$	$7.47.10^3$	$9.29.10^3$	$1.15.10^4$
ΔG (kJ mol^{-1})	−20.33	−21.28	−22.21	−23.21	−24.16	−25.11
ΔH^o (kJ mol^{-1})	30.4	-	-	-	-	-
ΔS^o (J K^{-1} mol^{-1})	177	-	-	-	-	-
R^2	0.9998	-	-	-	-	-
RR-120						
CC-1.9						
K_g (L mol^{-1})	$2.70.10^4$	$3.09.10^4$	$3.43.10^4$	$3.96.10^4$	$4.46.10^4$	$5.03.10^4$
ΔG (kJ mol^{-1})	−25.28	−26.04	−26.74	−27.55	−28.30	−29.07
ΔH^o (kJ mol^{-1})	19.9	-	-	-	-	-
ΔS^o (J K^{-1} mol^{-1})	151	-	-	-	-	-
R^2	0.9985	-	-	-	-	-
CC-2.2						
K_g (L mol^{-1})	$5.96.10^3$	$7.02.10^3$	$8.12.10^3$	$9.51.10^3$	$1.12.10^4$	$1.31.10^4$
ΔG (kJ mol^{-1})	−21.54	−22.31	−23.05	−23.84	−24.65	−25.46
ΔH^o (kJ mol^{-1})	25.2	-	-	-	-	-
ΔS^o (J K^{-1} mol^{-1})	157	-	-	-	-	-
R^2	0.9988	-	-	-	-	-

different adsorbents for treatment of simulated dye effluents [3,13, 14,18,21,22]. It is possible to deduce, based on the simulated effluent data, that both carbon adsorbents are efficient and effective for the treatment of real wastewater effluents.

CONCLUSION

Carbon composite materials CC-1.9 and CC-2.2 are good alternative adsorbents for removal of the textile dyes, RO-16 and RR-120, from aqueous solutions. The maximum amounts of dyes adsorbed at 323 K were 144.8 (CC-1.9) and 139.5 mg g^{-1} (CC-2.2) for RO-16 dye and 95.76 (CC-1.9) and 93.80 mg g^{-1} for RR-120 dye. For RO-16 dye, the kinetic was faster and the maximum amount adsorbed on CC-1.9 and CC-2.2 was higher when compared to the RR-120 dye. This better adsorption efficiency for the RO-16 dye in relation to the RR-120 dye was attributed to the lower dimension of RO-16.

ACKNOWLEDGEMENTS

We are grateful to Centro de Microscopia Eletrônica (CME-UFRGS) for the use of the SEM microscope. The authors are grateful to CNPq, CAPES and TWAS for financial support and fellowships.

REFERENCES

1. C. Hessel, C. Allegre, M. Maisseu, F. Charbit and P Moulin, *J. Environ. Manage.*, **83**, 171 (2007).
2. C. Allègre, P. Moulin, M. Maisseu and F. Charbit, *J. Membr. Sci.*, **269**, 15 (2006).
3. N. F. Cardoso, E. C. Lima, B. Royer, M. V. Bach, G. L. Dotto, L. A. A. Pinto and T. Calvete, *J. Hazard. Mater.*, **241-242**, 146 (2012).
4. L.G. da Silva, R. Ruggiero, P. M. Gontijo, R. B. Pinto, B. Royer, E. C. Lima, T. H. M. Fernandes and T. Calvete, *Chem. Eng. J.*, **168**, 620 (2011).
5. D. S. Brookstein, *Dermatol. Clin.*, **27**, 309 (2009).
6. R. O. A. de Lima, A. P. Bazo, D. M. F. Salvadori, C. M. Rech, D. P. Oliveira and G. A. Umbuzeiro, *Mutat. Res. Genet. Toxicol. Environ. Mutagen.*, **626**, 53 (2007).
7. P. A. Carneiro, G. A. Umbuzeiro, D. P. Oliveira and M. V. B. Zanoni, *J. Hazard. Mater.*, **174**, 694 (2010).
8. M. Oplatowska, R. F. Donnelly, R. J. Majithiya, D. G. Kennedy and C. T. Elliott, *Food Chem. Toxicol.*, **49**, 1870 (2011).
9. H. Ali, *Water Air Soil Pollut.*, **213**, 251 (2010).
10. S. Alijani, A. Z. Moghaddam, M. Vaez and J. Towfighi, *Korean J. Chem. Eng.*, **30**, 1855 (2013).
11. B. Royer, N. F. Cardoso, E. C. Lima, T. R. Macedo and C. Airoldi,

J. Hazard. Mater., **181**, 366 (2010).
12. B. Royer, N. F. Cardoso, E. C. Lima, V. S. O. Ruiz, T. R. Macedo and C. Airoldi, *J. Colloid Interface Sci.*, **336**, 398 (2009).
13. E. W. de Menezes, E. C. Lima, B. Royer, F. E. de Souza, B. D. dos Santos, J. R. Gregório, T. M. H. Costa, Y. Gushikem and E. V. Benvenutti, *J. Colloid Interface Sci.*, **378**, 10 (2012).
14. L. D. T. Prola, E. Acayanka, E. C. Lima, C. S. Umpierres, J. C. P. Vaghetti, W. O. Santos, S. Laminsi and P. T. Njifon, *Ind. Crop Prod.*, **46**, 328 (2013).
15. G. L. Dotto, E. C. Lima and L. A. A. Pinto, *Bioresour. Technol.*, **103**, 123 (2012).
16. S. Nethaji, A. Sivasamy and A. B. Mandal, *Int. J. Environ. Sci. Technol.*, **10**, 231 (2013).
17. P. Sharma, H. Kaur, M. Sharma and V. Sahore, *Environ. Monit. Assess*., **183**, 151 (2011).
18. L. D. T. Prola, F. M. Machado, C. P. Bergmann, F. E. de Souza, C. R. Gally, E. C. Lima, M. A. Adebayo, S. L. P. Dias and T. Calvete, *J. Environ. Manage.*, **130**, 166 (2013).
19. N. F. Cardoso, E. C. Lima, I. S. Pinto, C. V. Amavisca, B. Royer, R. B. Pinto, W. S. Alencar and S. F. P. Pereira, *J. Environ. Manage.*, **92**, 1237 (2011).
20. L. D. T. Prola, E. Acayanka, E. C. Lima, C. Bestetti, W. O. Santos, F. A. Pavan, S. L. P. Dias and C. R. T. Tarley, *Desalin. Water Treat.*, **51**, 4582 (2013).
21. F. M. Machado, C. P. Bergmann, T. H. M. Fernandes, E. C. Lima, B. Royer, T. Calvete and S. B. Fagan, *J. Hazard. Mater.*, **192**, 1122 (2011).
22. W. S. Alencar, E. C. Lima, B. Royer, B. D. dos Santos, T. Calvete, E. A. da Silva and C. N. Alves, *Sep. Sci. Technol.*, **47**, 513 (2012).
23. T. Calvete, E. C. Lima, N. F. Cardoso, J. C. P. Vaghetti, S. L. P. Dias and F. A. Pavan, *J. Environ. Manage.*, **91**, 1695 (2010).
24. H. Marsh and F. R. Reinoso, *Activated Carbon*, Elsevier, Amsterdam (2006).
25. T. Mitome, Y. Uchida, Y. Egashira, K. Hayashi, A. Nishiura and N. Nishiyama, *Colloids Surf. A*, **424**, 89 (2013).
26. Ö. Şahin and C. Saka, *Bioresour. Technol.*, **136**, 163 (2013).
27. J. Kong, Q. Yue, L. Huang, Y. Gao, Y. Sun, B. Gao, Q. Li and Y. Wang, *Chem. Eng. J.*, **221**, 62 (2013).
28. Q. Wang, Z. Luan, N. Wei, J. Li and C. Liu, *J. Hazard. Mater.*, **170**, 690 (2009).
29. E. B. da Silva-Filho, M. C. M. Alves, M. da Motta, E. H. C. Oliveira and W. Brander-Jr, *Quim. Nova*, **31**, 985 (2008).
30. K. C. de Souza, M. L. P. Antunes, S. J. Couperthwaite, F. T. da Conceição, T. R. de Barros and R. Frost, *J. Colloid Interface Sci.*, **396**, 210 (2013).
31. A. Tor and Y. Cengeloglu, *J. Hazard. Mater.*, **138**, 409 (2006).
32. R. A. C. Mártires, Sumário Mineral 2012. *Departamento Nacional de Produção Mineral*. Brasil (2012).
33. P. S. Tully, Sulfonic acids. *Kirk-Othmer Encyclopedia of Chemical Technology*, John Wiley and Sons, New Jersey (2000).
34. R. A. Jacques, E. C. Lima, S. L. P. Dias, A. C. Mazzocato and F. A. Pavan, *Sep. Purif. Technol.*, **57**, 193 (2007).
35. R. A. Jacques, R. Bernardi, M. Caovila, E. C. Lima, F. A. Pavan, J. C. P. Vaghetti and C. Airoldi, *Sep. Sci. Technol.*, **42**, 591 (2007).
36. J. C. P. Vaghetti, M. Zat, K. R. S. Bentes, L. S. Ferreira, E. V. Benvenutti and E. C. Lima, *J. Anal. Atom. Spectrom.*, **18**, 376 (2003).
37. F. Barbosa-Jr., F. J. Krug and E. C. Lima, *Spectrochim. Acta B*, **54**, 1155 (1999).
38. E. C. Lima, J. L. Brasil and A. H. D. P. Santos, *Anal. Chim. Acta*, **484**, 233 (2003).
39. E. C. Lima, F. J. Krug, J. A. Nobrega and A. R. A. Nogueira, *Talanta*, **47**, 613 (1998).
40. E. C. Lima, P. G. Fenga, J. R. Romero and W. F. de Giovani, *Polyhedron*, **17**, 313 (1998).
41. Y. Liu and Y. J. Liu, *Sep. Purif. Technol.*, **61**, 229 (2008).
42. Y. Liu and L. Shen, *Biochem. Eng. J.*, **38**, 390 (2008).
43. Y. S. Ho, *J. Hazard. Mater.*, **136**, 681 (2006).
44. W. J. Weber-Jr. and J. C. Morris, *J. Sanit. Eng. Div. Am. Soc. Civil Eng.*, **89**, 31 (1963).
45. I. Langmuir, *J. Am. Chem. Soc.*, **40**, 1361 (1918).
46. H. Freundlich, *Phys. Chem. Soc.*, **40**, 1361 (1906).
47. Y. Liu, H. Xu, S. F. Yang and J. H. Tay, *J. Biotechnol.*, **102**, 233 (2003).
48. M. I. El-Khaiary and G. F. Malash, *Hydrometallurgy*, **105**, 314 (2011).
49. V. K. Gpta, and A. Nayak, *Chem. Eng. J.*, **180**, 81 (2012).
50. P. Suksabye and P. Thiravetyan, *J. Environ. Manage.*, **102**, 1 (2012).
51. J. Zhang, Q. Ping, M. Niu, H. Shi and N. Li, *Appl. Clay Sci.*, **83-84**, 12 (2013).
52. C. L. Sun and C. S. Wang, *J. Mol. Struct.*, **956**, 38 (2010).
53. G. Z. Kyzas, N. K. Lazaridis and D. N. Bikiaris, *Carbohyrd. Polym.*, **91**, 198 (2013).
54. N. A. Travlou, G. Z. Kyzas, N. K. Lazaridis and E. A. Deliyanni, *Chem. Eng. J.*, **217**, 256 (2013).

Supporting Information

New carbon composite adsorbents for the removal of textile dyes from aqueous solutions : Kinetic, equilibrium, and thermodynamic studies

Davis Castro dos Santos*, Matthew Ayorinde Adebayo,***, Simone de Fátima Pinheiro Pereira*, Lizie Daniela Tentler Prola**, Renato Cataluña**, Eder Cláudio Lima*,†, Caroline Saucier**, Caline Rodrigues Gally**, and Fernando Machado Machado******

*Institute of Exact and Natural Sciences, Federal University of Para, UFPA, Belem, PA, Brazil
**Institute of Chemistry, Federal University of Rio Grande do Sul, UFRGS, Av. Bento Gonçalves 9500, Postal Box 15003, ZIP 91501-970, Porto Alegre, RS, Brazil
***Department of Chemical Sciences, Ajayi Crowther University, PMB 1066, Oyo, Oyo State, Nigeria
****Universitary Center Franciscano, UNIFRA, R. dos Andradas 1614, ZIP 97010-032, Santa Maria, RS, Brazil
(*Received 9 January 2014 • accepted 18 March 2014*)

5. Kinetic Adsorption Models

In a chemical reaction or process, rate law's exponents are generally unrelated to the chemical equation's coefficients, but they are sometimes the same by coincidence. This means that there is no way to predict the reaction order without experimental data. In order to establish the general rate law equation for adsorption, the adsorption process on the surface of adsorbent is assumed to be rate controlling step [41,42]. In this case, attention is shifted from adsorbate concentration in bulk solution to change in the effective number of adsorption sites at the surface of adsorbent during adsorption. If the reaction rate law is applied to Eq. (1), rate expression for adsorption can be obtained as follows:

$$\frac{dq}{dt} = k_N(q_e - q_t)^n \quad (1)$$

in which k_N is the rate constant and n is the adsorption reaction order

Supplementary Table 1. Kinetic parameters for RO-16 and RR-120 removal using CC-1.9 and CC-2.2 as adsorbents. Conditions: temperature was fixed at 298 K; pH 2.0, mass of adsorbent 50.0 mg

	CC-1.9				CC-2.2			
	RO-16		RR-120		RO-16		RR-120	
	50.0 mg L^{-1}	100.0 mg L^{-1}	50.0 mg L^{-1}	100.0 mg L^{-1}	50.0 mg L^{-1}	100.0 mg L^{-1}	50.0 mg L^{-1}	100.0 mg L^{-1}
Pseudo-first-order								
k_f (h^{-1})	3.131	3.144	1.208	1.176	3.017	3.148	1.077	1.129
q_e (mg g^{-1})	17.96	28.95	17.06	29.09	17.42	28.58	17.35	28.04
h_o (mg g^{-1} h^{-1})	56.22	91.01	20.61	34.21	52.57	89.96	18.69	31.67
R^2_{adj}	0.9898	0.9876	0.9969	0.9983	0.9903	0.9874	0.9978	0.9992
F_{error} (mg g^{-1})	0.5281	0.9329	0.3326	0.4214	0.5020	0.9304	0.2990	0.2782
Pseudo-second-order								
k_s (g mg^{-1} h^{-1})	0.2497	0.1558	0.07776	0.04400	0.2461	0.1579	0.06529	0.04326
q_e (mg g^{-1})	19.11	30.82	19.22	32.84	18.57	30.43	19.76	31.76
h_o (mg g^{-1} h^{-1})	91.28	147.9	28.73	47.45	84.89	146.2	25.49	43.65
R^2_{adj}	0.9966	0.9979	0.9951	0.9932	0.9967	0.9980	0.9924	0.9918
F_{error} (mg g^{-1})	0.3045	0.3862	0.4215	0.8547	0.2948	0.3664	0.5501	0.9083
General order								
k_N [$h^{-1} \cdot (g\ mg^{-1})^{n-1}$]	0.7979	0.4832	0.5445	0.6074	0.8006	0.4746	0.6462	0.7185
q_e (mg g^{-1})	18.46	29.92	17.52	29.59	17.90	29.56	17.65	28.37
N	1.558	1.638	1.315	1.217	1.548	1.646	1.201	1.151
h_0 (mg g^{-1} h^{-1})	75.02	126.2	23.49	37.53	69.63	125.3	20.32	33.80
R^2_{adj}	0.9998	0.9999	0.9998	0.9998	0.9999	0.9999	0.9989	0.9996
F_{error} (mg g^{-1})	0.07913	0.3862	0.09527	0.1628	0.04013	0.07410	0.2084	0.06688
Intra-particle diffusion								
$k_{id,2}$ (mg g^{-1} $h^{-0.5}$)[a]	2.207	2.282	3.125	8.245	3.539	5.511	4.687	5.327

[a]Second stage

Supplementary Table 2. Isotherm parameters for RO-16 and RR-120 adsorption, using CC-1.9 and CC-2.2 adsorbents. Conditions: initial pH 2.0; adsorbent mass 50.0 mg, time of contact between the adsorbent and adsorbate were 5.0 h for RO-16 and 6.0 h for RR-120 dye

	CC-1.9						CC-2.2					
	298 K	303 K	308 K	313 K	318 K	323 K	298 K	303 K	308 K	313 K	318 K	323 K
RO-16												
Langmuir												
Q_{max} (mg g^{-1})	43.87	53.13	75.57	117.7	188.5	230.4	42.89	46.49	54.59	64.27	73.94	81.37
K_L (L mg^{-1})	0.1189	0.05535	0.02327	0.01206	0.007390	0.007450	0.1304	0.1947	0.1395	0.1086	0.1048	0.1333
R^2_{adj}	0.9594	0.9834	0.9964	0.9999	0.9987	0.9964	0.9695	0.9521	0.9647	0.9702	0.9744	0.9684
F_{error} (mg g^{-1})	2.638	1.846	1.056	0.2432	0.9863	1.989	1.985	3.140	3.137	3.338	3.502	4.246
Freudlich												
K_F (mg g^{-1} (mg L^{-1})$^{-1/nF}$)	11.56	8.114	4.842	3.275	2.655	3.271	13.45	15.05	14.95	15.76	18.34	24.07
n_F	3.464	2.564	1.880	1.528	1.340	1.342	3.969	3.908	3.499	3.287	3.333	3.766
R^2_{adj}	0.9973	0.9971	0.9960	0.9936	0.9918	0.9870	0.9984	0.9974	0.9969	0.9959	0.9953	0.9949
F_{error} (mg g^{-1})	0.6756	0.7755	1.115	1.773	2.431	3.767	0.4551	0.7280	0.9325	1.244	1.511	1.706
Liu												
Q_{max} (mg g^{-1})	97.42	105.4	114.0	124.2	134.5	144.8	93.50	100.8	109.8	118.7	128.8	139.5
K_g (L mg^{-1})	0.005680	0.007040	0.008790	0.01082	0.01348	0.01687	0.006090	0.007760	0.009710	0.01242	0.01544	0.01915
n_L	0.4153	0.5527	0.7582	0.9696	1.189	1.320	0.3807	0.3801	0.4309	0.4721	0.4833	0.4461
R^2_{adj}	0.9998	0.9998	0.9999	0.9999	0.9999	0.9999	0.9999	0.9999	0.9999	0.9999	0.9999	0.9999
F_{error} (mg g^{-1})	0.2047	0.1951	0.2003	0.1965	0.2260	0.3563	0.1327	0.1194	0.09218	0.1134	0.1430	0.2183
RR-120												
Langmuir												
Q_{max} (mg g^{-1})	48.69	52.56	56.10	58.79	59.30	61.96	42.55	43.06	43.24	44.68	47.90	49.41
K_L (L mg^{-1})	0.07248	0.07292	0.07761	0.09517	0.1435	0.1776	0.1454	0.2587	0.4565	1.316	2.332	12.17
R^2_{adj}	0.9730	0.9769	0.9802	0.9738	0.9639	0.9578	0.9536	0.9364	0.9225	0.9073	0.9107	0.8629
F_{error} (mg g^{-1})	2.5475	2.516	2.391	2.848	3.470	3.864	2.701	3.193	3.581	3.975	4.207	5.595
Freudlich												
K_F (mg g^{-1} (mg L^{-1})$^{-1/nF}$)	11.68	11.46	12.68	15.27	18.03	21.45	14.25	18.22	20.96	26.96	30.57	33.56
n_F	3.597	3.301	3.346	3.650	3.983	4.421	4.362	5.397	6.189	8.409	9.208	9.949
R^2_{adj}	0.9898	0.9895	0.9907	0.9906	0.9914	0.9923	0.9937	0.9954	0.9959	0.9978	0.9981	0.9972
F_{error} (mg g^{-1})	1.567	1.699	1.636	1.705	1.696	1.645	0.9928	0.8548	0.8258	0.6071	0.6212	0.8017
Liu												
Q_{max} (mg g^{-1})	73.82	77.33	81.58	85.95	90.64	95.76	72.02	75.00	77.00	82.81	89.07	93.80
K_g (L mg^{-1})	0.01840	0.02101	0.02332	0.02691	0.03032	0.03421	0.01935	0.02280	0.02635	0.03088	0.03634	0.04261
n_L	0.4968	0.5459	0.5523	0.5232	0.4747	0.4350	0.4088	0.3386	0.2957	0.2188	0.2010	0.1830
R^2_{adj}	0.9999	0.9997	0.9998	0.9999	0.9998	0.9999	0.9999	0.9999	0.9999	0.9999	0.9999	0.9999
F_{error} (mg g^{-1})	0.1843	0.2821	0.2063	0.2041	0.2313	0.2081	0.1279	0.1496	0.1531	0.1189	0.05451	0.1088

with regard to the effective concentration of the adsorption sites available on the surface of adsorbent, q_e is the amount adsorbed at the equilibrium and q_t is the amount adsorbed at any time. Eq. (1) is the result of application of the universal rate law to adsorption process, and can be used without any further assumption. Theoretically, the exponent n in Eq. (1) can be integral or rational non-integral numbers [41,42].

Eq. (2) defines the available number of the adsorption sites (θ_t) on the surface of adsorbent [41,42].

$$\theta_t = 1 - \frac{q_t}{q_e} \tag{2}$$

Eq. (3) describes the rate of adsorption in function of variable (θ_t).

$$\frac{d\theta_t}{dt} = -k\theta_t^n \tag{3}$$

Where $k = k_N (q_e)^{n-1}$

For a virgin adsorbent, θ_t equals 1 and tends to decrease during adsorption process. When adsorption process reaches equilibrium, θ_t tends to a fixed value. If the saturation of the adsorbent occurs, θ_t will become zero (22).

Integration of Eq. (3) results in Eq. (4):

$$\int_1^{\theta} \frac{d\theta_t}{\theta_t^n} = -k\int_0^t dt \tag{4}$$

Eq. (4) leads to:

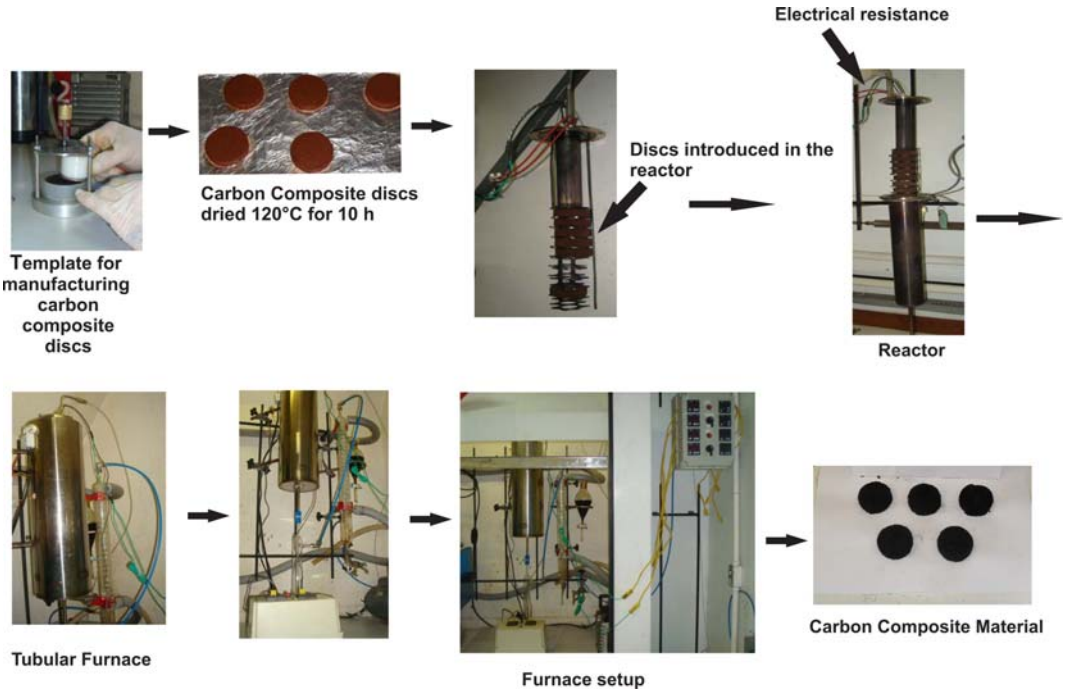

Supplementary Fig. 1. Production of carbon composite adsorbents.

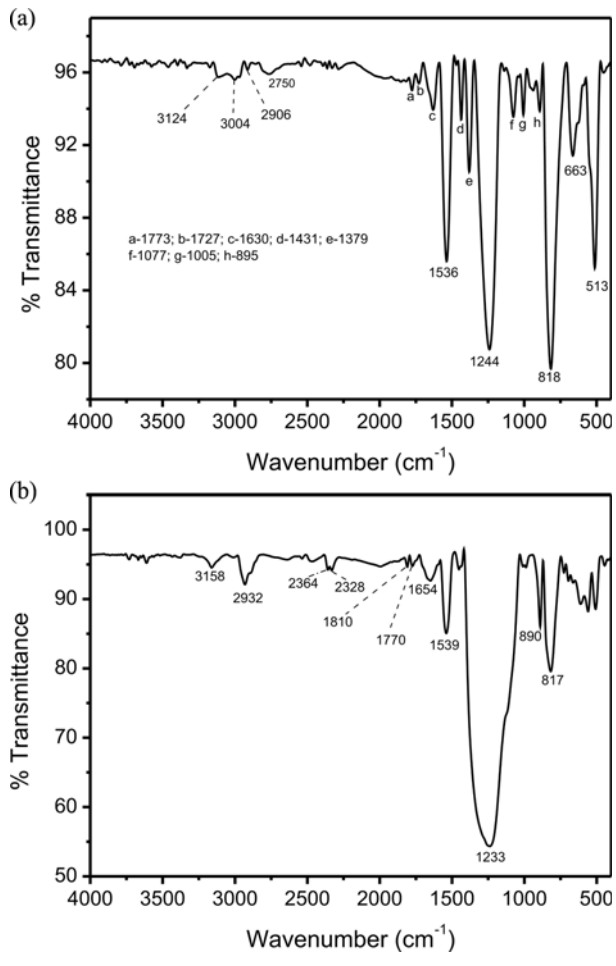

Supplementary Fig. 2. FTIR of: (a) CC-1.9 and (b) CC-2.2.

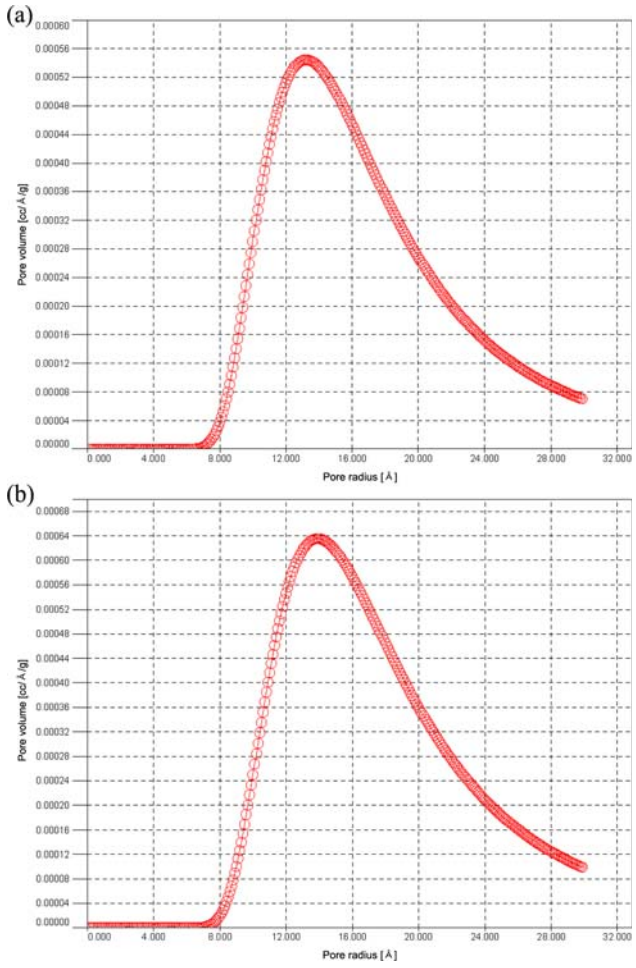

Supplementary Fig. 3. NLDFT pore radius distribution of CC-1.9 (a) and CC-2.2 (b).

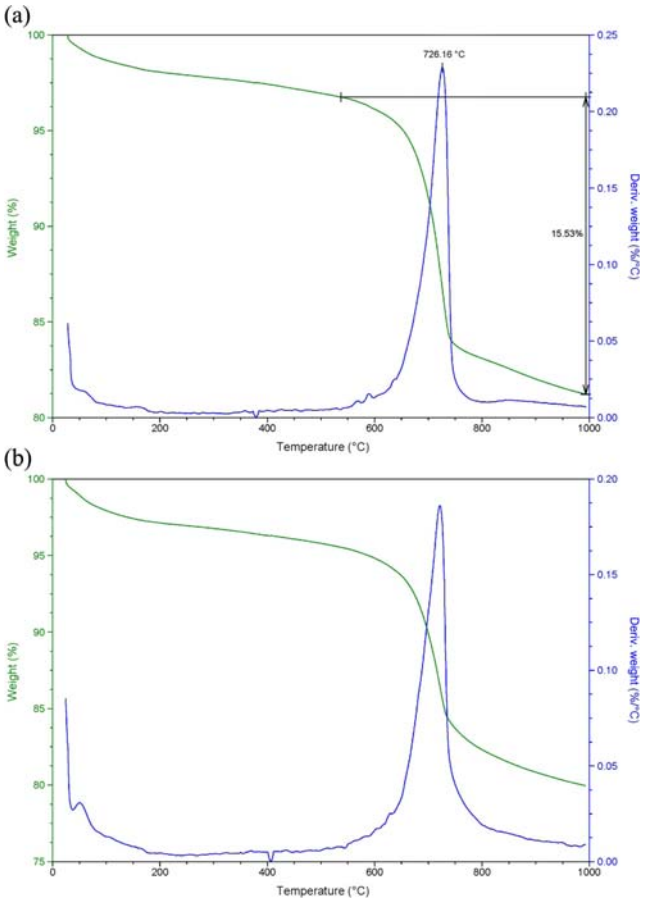

Supplementary Fig. 4. TGA and DTG curves of (a) CC-1.9 and (b) CC-2.2 adsorbents.

$$\frac{1}{1-n}\cdot[\theta_t^{1-n}-1]=-kt \tag{5}$$

This results in:

$$\theta_t=[1-k(1-n)\cdot t]^{1/1-n} \tag{6}$$

Applying the definition of parameter k given by $k=k_N(q_e)^{n-1}$ and substitute Eq. (2) into Eq. (6), Eq. (7) is obtained.

$$q_t=q_e-\frac{q_e}{[k_N(q_e)^{n-1}\cdot t\cdot(n-1)+1]^{1/1-n}} \tag{7}$$

Eq. (7) is the General kinetic adsorption equation that is valid for $n\neq1$ (22).

The pseudo-first order kinetic model is a special case of Eq. (3), when n=1 [41,42].

$$\frac{d\theta_t}{dt}=-k\cdot\theta_t^1 \tag{8}$$

Integrating Eq. (8) gives Eq. (9):

$$\theta_t=\exp(-k_1\cdot t) \tag{9}$$

Substituting Eq. (2) into Eq. (9) and put $k=k_1$, pseudo-first order kinetic model is obtained.

$$q_t=q_e[1-\exp(-k_1\cdot t)] \tag{10}$$

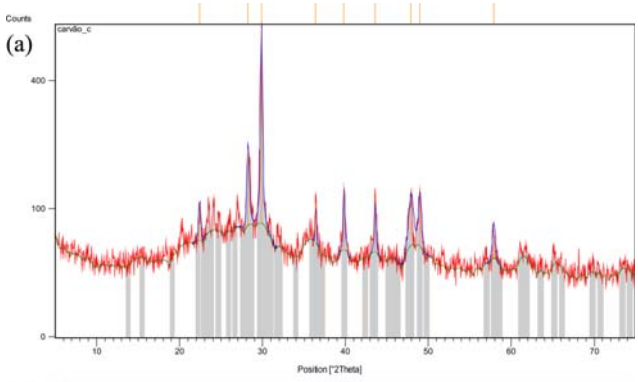

(b)

Pos. [°2Th.]	Height [cts]	FWHM [°2Th.]	d-spacing [Å]	Rel. Int. [%]
22.4008	51.13	0.2952	3.96897	10.19
28.2090	140.69	0.2952	3.16358	28.04
29.8356	501.74	0.2460	2.99471	100.00
36.4164	54.45	0.1476	2.46723	10.85
39.8328	94.15	0.1968	2.26314	18.76
43.5866	72.83	0.1968	2.07655	14.52
47.9110	67.98	0.5904	1.89873	13.55
48.9796	72.85	0.3936	1.85978	14.52
57.8675	30.94	0.3600	1.59219	6.17

(c)

Ref. Code	Score	Compound Name	Displacement [°2Th.]	Scale Factor	Chemical Formula
00-052-1344	21	Calcium Aluminum Silicate	0.157	0.163	$Ca_{0.88}S_{0.12}$ $Al_{1.77}$ $Si_{2.23}O_8$
00-005-0586	67	Calcite.syn.	0.419	0.984	$CaCO_3$

Supplementary Fig. 5. X-ray difractogram of CC-1.9.

Therefore, the pseudo-first order kinetic equation is a special case of general kinetic adsorption.

The pseudo-second order kinetic model [43] is a special case of Eq. (7) (General order kinetic equation), when n=2. Therefore,

$$q_t=q_e-\frac{q_e}{[k_2(q_e)\cdot t+1]} \tag{11}$$

Rearrangement of Eq. (11) leads to Eq. (12).

$$q_t=\frac{q_e^2k_2t}{[k_2(q_e)\cdot t+1]} \tag{12}$$

The *Intra-particle diffusion equation* [44] was early defined as Eq. (13).

$$q_t=k_{id}\sqrt{t}+C \tag{13}$$

Where k_{id} is the intra-particle diffusion rate constant (mg g^{-1} $h^{-0.5}$); C is a constant related with the thickness of boundary layer (mg g^{-1}).

In this work the pseudo-first order (Eq. (10)), pseudo-second order (Eq. (12)), general order equation (Eq. (7)) and intra-particle diffusion (Eq. (13)) models were utilised for evaluation the kinetics of adsorption of the dye on the adsorbents.

6. Equilibrium Models

The equilibrium of adsorption was evaluated by using the following isotherm models.

Langmuir Isotherm model [45]:

$$q_e=\frac{Q_{max}\cdot K_L\cdot C_e}{1+K_L\cdot C_e} \tag{14}$$

Where q_e is amount adsorbate adsorbed at the equilibrium (mg g^{-1}); Q_{max} is the maximum adsorption capacity of the adsorbent (mg g^{-1}); K_L is the Langmuir equilibrium constant (L mg^{-1}); C_e is dye concentration at the equilibrium (mg L^{-1}).

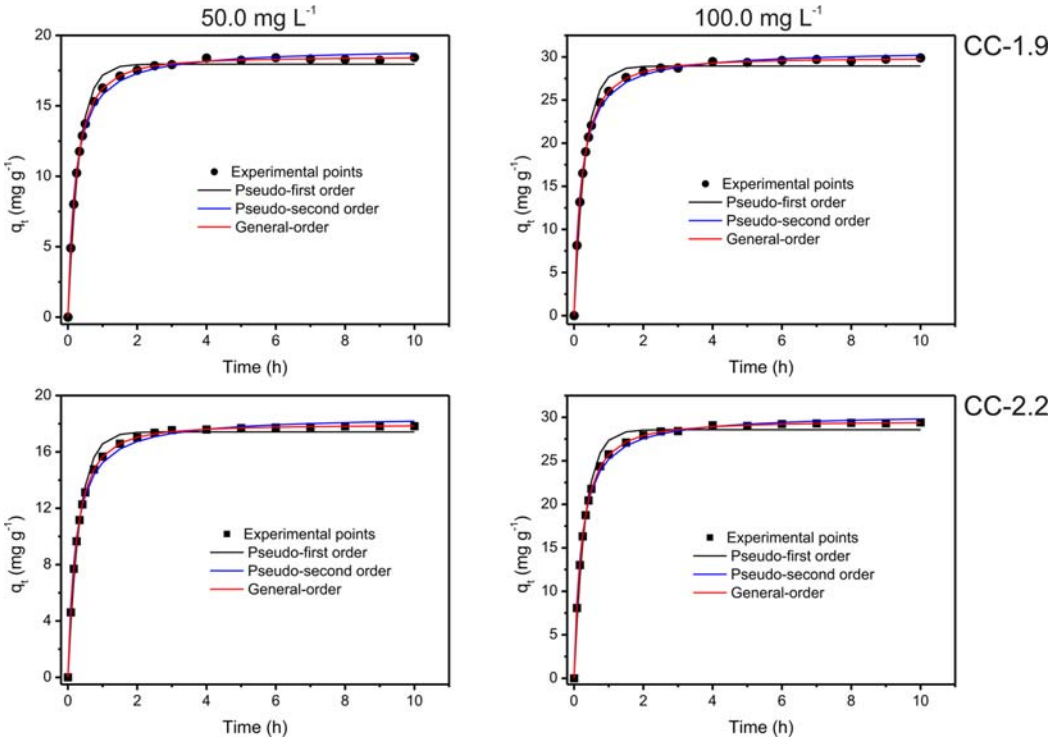

Supplementary Fig. 6. Kinetic isotherm curves for RO-16 dye. Conditions: initial pH 2.0; temperature 298 K; adsorbent mass 50.0 mg.

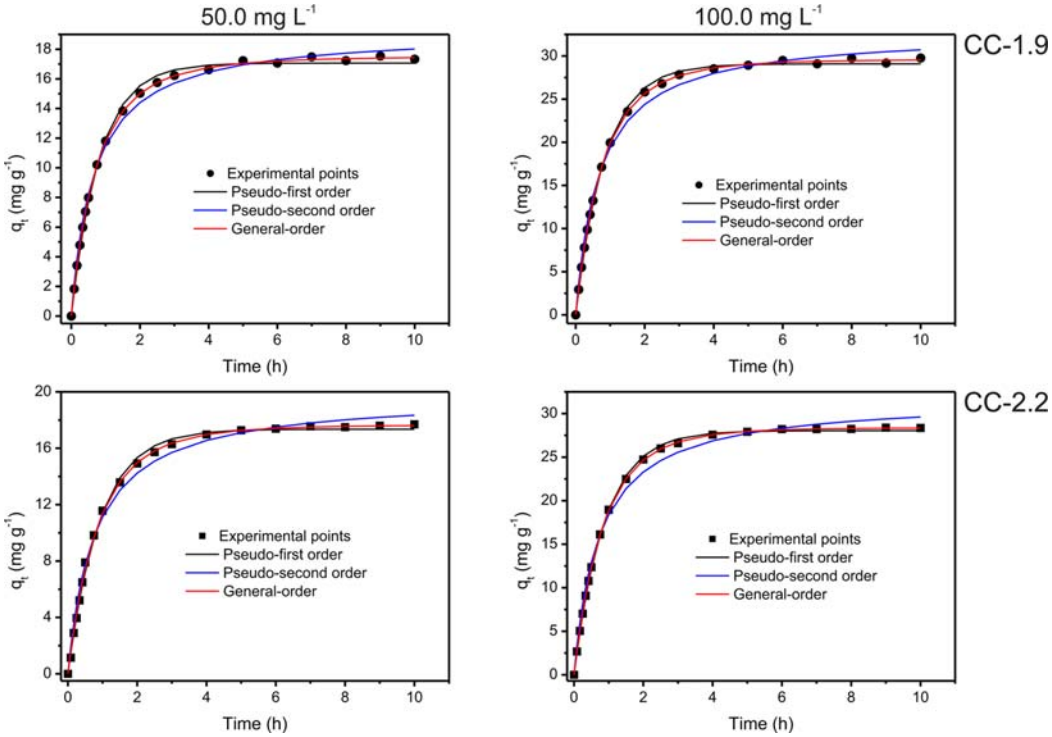

Supplementary Fig. 7. Kinetic isotherm curves for RR-120 dye. Conditions: initial pH 2.0; temperature 298 K; adsorbent mass 50.0 mg.

Freundlich isotherm model [46]:

$$q_e = K_F \cdot C_e^{1/n_F} \quad (15)$$

Where K_F is the Freundlich equilibrium constant [mg g^{-1} (mg L^{-1})$^{-1/n_F}$]; n_F is dimensionless exponent of the Freundlich equation.

Liu isotherm model [47].

$$q_e = \frac{Q_{max} \cdot (K_g \cdot C_e)^{n_L}}{1 + (K_g \cdot C_e)^{n_L}} \quad (16)$$

Where Q_{max} is the maximum adsorption capacity of the biosorbent

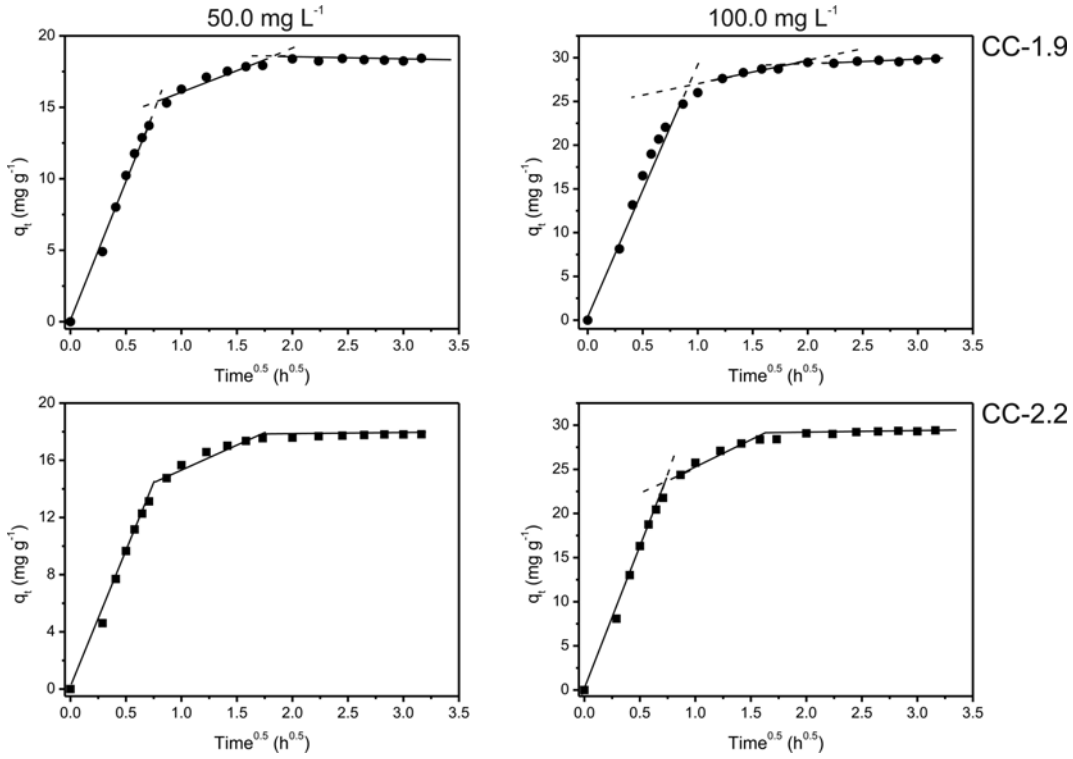

Supplementary Fig. 8. Intra-particle diffusion graphs of RO-16.

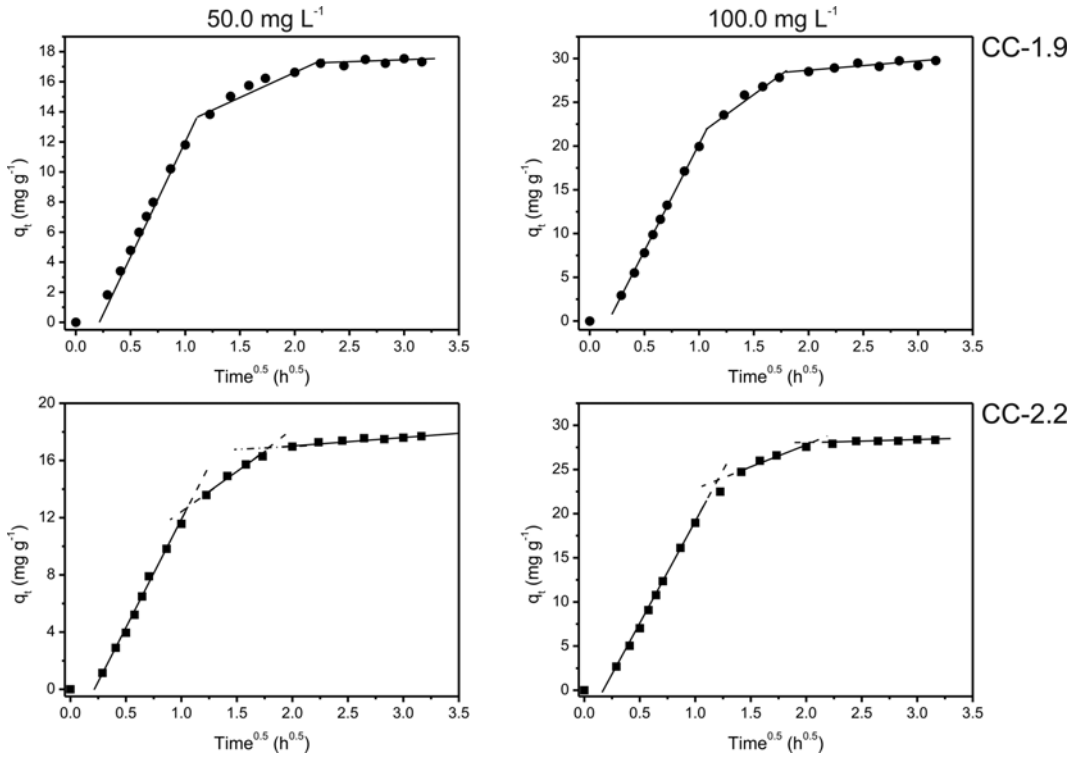

Supplementary Fig. 9. Intra-particle diffusion graphs of RR-120.

(mg g^{-1}), K_g is the Liu equilibrium constant (L mg^{-1}); n_L is dimensionless exponent of the Liu equation; C_e is dye concentration at the equilibrium (mg L^{-1}).

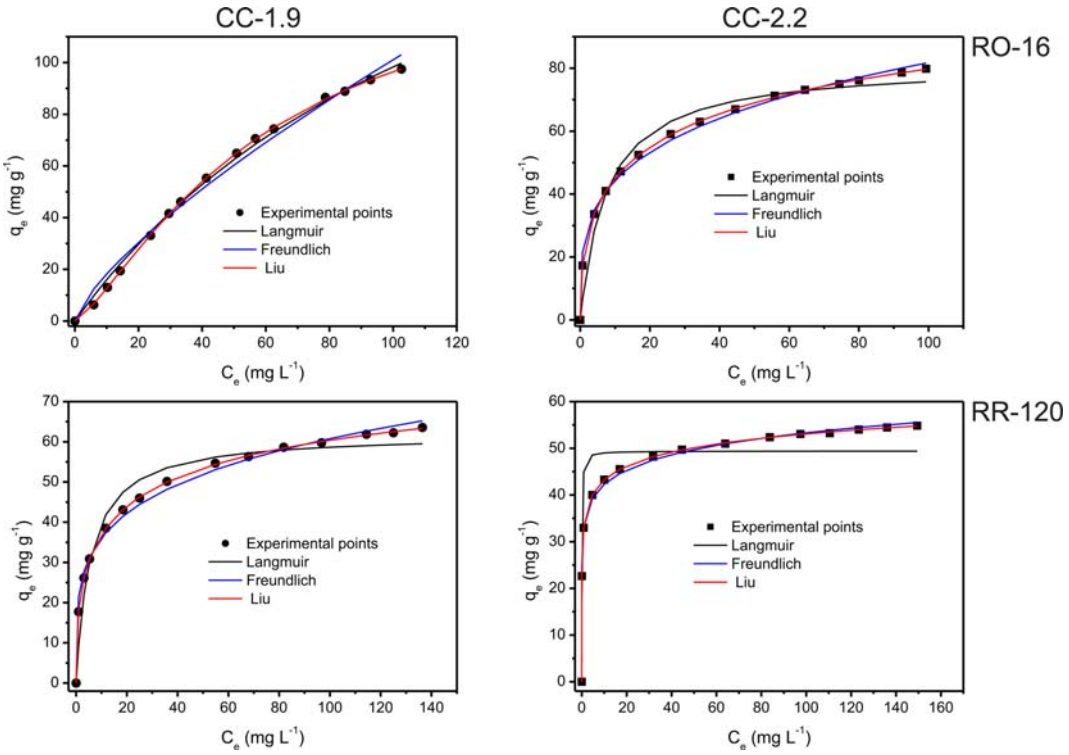

Supplementary Fig. 10. Isotherm curves of RO-16 and RR-120 dyes on CC-1.9 and CC-2.2 adsorbents at 323 K. Conditions: initial pH 2.0; adsorbent mass 50.0 mg, time of contact between the adsorbent and adsorbate were 5.0 h for RO-16 and 6.0 h for RR-120 dye.